Letter

Controllable operations of edge states in cross-one-dimensional topological chains

Xian-Liang Lu [1,2] and Ze-Liang Xiang [1,3,*]

[1] *School of Physics, Sun Yat-sen University, Guangzhou 510275, China*

[2] *Department of Physics, University of Colorado, Boulder, Colorado 80309, USA*

[3] *State Key Laboratory of Optoelectronic Materials and Technologies, Sun Yat-sen University, Guangzhou 510275, China*

(Received 14 August 2023; accepted 1 November 2025; published 3 December 2025)

Topological edge states have recently attracted intense interest due to their robustness in the presence of disorder and defects. However, most approaches for manipulating such states require global modulations of the system's Hamiltonian. In this work, we develop a method to control edge states using local interactions of a four-node junction between cross-one-dimensional topological atomic chains. These junction interactions can give rise to tunable couplings between the hybridized edge states within different geometric symmetries, allowing us to implement robust quantum state transfer and SWAP gate between the two topological chains via a double-quench protocol. Moreover, when the atoms in chains are precisely positioned and coupled to waveguides, the correlated decay caused by the environment enables the symmetric edge states to present subradiant dynamics and thus show extremely long coherence time. These findings open up possibilities for future quantum technologies with topological edge states.

DOI: 10.1103/ylrq-98wl

As a fundamental element in topological materials, the edge states predicted by the bulk-boundary correspondence emerge at the interface where the topological invariant changes [1,2]. One of the most significant features of topological systems is their robustness against disorder and defects [3–5], which leads to topologically protected energy and information flow [6–8]. In addition, the zero-energy edge states [9] in the one-dimensional (1D) topological system with chiral Hamiltonian can separate from bulk states with large band gaps [10,11]. These unique advantages show great potential in realizing robust quantum state transfer with 1D lattices [12–18], as well as performing topological quantum computation in superconducting wire networks [19–21], where the unpaired Majorana zero modes are encoded as qubits. Thus, achieving the quantum control of such topological edge states has become a critical issue.

The transfer and operations of multiple protected edge states are vital in robust quantum computation and large-scale quantum information processing. Previous works have developed techniques based on adiabatic protocols to drive single edge state [15–18,22–24], in which the operation time is generally limited by the adiabatic theorem without accelerated strategies [17]. The topological charge pump, introduced by Thouless [25], can give rise to a quantized transport of particles in each cyclic evolution [26,27]. In recent studies, nonquantized topological pumping is exploited to transfer the edge states [28,29], and experimental realizations have been reported in a variety of platforms, including photonics [30–33], elastic lattices [34], magneto- and electromechanical systems [35,36], and acoustic structures [37–39]. However, due to the topological robustness, these approaches demand simultaneous modulations of system parameters to drive the edge states, and they are incapable of building multiqubit operations with edge states. On the other hand, the quantum gates based on braiding in topological chains also require adiabatic moving of domain walls [40,41]. However, these adiabatic operations are not robust to nonadiabatic effects and can lead to decoherence effects [42,43]. Thus, it is still challenging to implement direct quantum control of topological edge states with few-body interactions and through coherent evolution. All of these give rise to the following question: Can one build tunable interactions between edge states to implement such transport and quantum gates through dynamical evolution?

In this Letter, we present a concise approach to control the topological edge states with few-body local interactions, where we leverage the interactions within a four-node junction formed by two intersecting topological chains of two-level atoms, to implement direct manipulations of edge states. In the topologically nontrivial phase, the paired zero-energy edge states [10,44] emerge at four edges of the system and are effectively controlled by the local junction interactions. When we encode the four edge states as two-qubit states, we find that the D_4 and D_2 geometric symmetries of the system can contribute to different qubit-qubit interactions, enabling us to implement the robust state transfer and a topological SWAP gate via the coherent evolution. Edge-state operations are implemented via a double-quench protocol consisting of preparation, interaction-on, and interaction-off stages. Moreover, we study the dissipative dynamics of the edge states

[*] Contact author: xiangzliang@mail.sysu.edu.cn

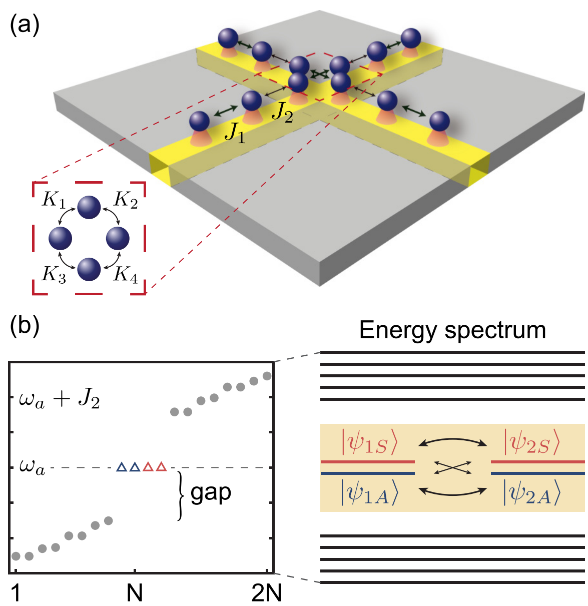

FIG. 1. (a) Schematic of the compound topological system. Two identical atomic chains with bipartite lattice have staggered hopping amplitudes J_1 and J_2, respectively, and there are tunable interchain hoppings K_i at the central node. Each chain is coupled to an individual waveguide. (b) Eigenenergies of the model (with an ω_a frequency shift) and the zero-energy manifold composed of the hybridized edge states in the single-excitation subspace. The interactions between edge states are mediated by tunable central network couplings K_i.

when the atoms in each topological chain are precisely positioned and coupled to 1D electromagnetic environment, which leads to the topologically protected super/subradiance of edge states. This allows us to generate and transfer remote entanglement between edge atoms. Our proposal provides a means of manipulating edge states via local interactions and paves the way for robust qubit operations as well as long-time storage.

Model. We consider a topological system as depicted in Fig. 1(a), where two identical topological chains cross at their mutual center. Each chain consists of $2N$ identical two-level atoms to form a Su-Schrieffer-Heeger (SSH) model [45]; i.e., the atoms are located in two sets of sublattices with alternated hopping rates. In addition, each chain couples to a waveguide in order to induce nonlocal dissipative couplings between atoms. Such a configuration can be realized with artificial atomic systems, such as superconducting circuits [46,47]. The Hamiltonian of atomic chains reads $H_{\text{tot}} = H_0 + H_{\text{XSSH}} + H_I$, where $H_0 = \sum_{l=1,2}\sum_i \omega_a \sigma_{l,i}^+\sigma_{l,i}^-$ denotes the bare Hamiltonian with the transition frequency ω_a. H_{XSSH} describes the two chains with no interchain hopping as $H_{\text{XSSH}} = \sum_{l=1,2}\sum_i (J_1\sigma_{l,iA}^+\sigma_{l,iB}^- + J_2\sigma_{l,i+1A}^+\sigma_{l,iB}^- + \text{H.c.})$, where l is the chain's index, and $\sigma_{l,iA}^{+(-)}$ and $\sigma_{l,iB}^{+(-)}$ are the raising (lowering) operators for atoms in the corresponding sublattices A and B of the ith unit cell. The staggered nearest-neighbor hopping amplitudes J_1 and J_2 represent the inter- and intracell hoppings, respectively. The crossed SSH chains are protected by chiral symmetry, placing the Hamiltonian H_{XSSH} in the BDI symmetry class [48]. Therefore, they show robustness against disorder in nearest-neighbor hopping. In the single-excitation subspace, when $J_1 < J_2$, the paired edge states emerge at the two ends of each finite-sized SSH chain, which hybridize from $|\psi_L\rangle$ and $|\psi_R\rangle$ into the symmetric ($|\psi_S\rangle$) and antisymmetric ($|\psi_A\rangle$) edge states, with energies [44]

$$\epsilon_S = -\epsilon_A = (-1)^{N+1}\frac{J_2\sinh\lambda}{\sinh(N+1)\lambda}, \tag{1}$$

where λ is given by $\sinh(N\lambda)/\sinh[(N+1)\lambda] = J_1/J_2$. In the inset of Fig. 1(a), we show the configuration of the central four-node junction. The atomic emitters are coupled through tunable couplers, which contribute to the interactions between the two topological chains,

$$\begin{aligned} H_I = {}& \left(K_1\sigma_{1,s}^+ + K_2\sigma_{1,s+1}^+\right)\sigma_{2,s}^- + \text{H.c.} \\ & + \left(K_3\sigma_{1,s}^+ + K_4\sigma_{1,s+1}^+\right)\sigma_{2,s+1}^- + \text{H.c.}, \end{aligned} \tag{2}$$

where s and $s+1$ are the location index of central atoms. Without loss of generality [47], the cell number N is assumed to be odd and thus $s = \{(N+1)/2, A\}$, $s+1 = \{(N+1)/2, B\}$. The interaction contains edge-edge couplings, offering transition channels between these edge states, as illustrated in Fig. 1(b), whereas the bulk-edge transition is suppressed due to the large band gap Δ_{gap} between the edge and bulk states [11]. Additionally, this gap also protects the edge states from thermal noise below a critical temperature [49–51], allowing us to focus on the dynamics within the zero-energy manifold of edge states. When the interaction is switched on (first quench), the edge states lose their topological protection since H_I breaks the chiral symmetry. However, we consider H_I as a perturbation with $||H_I|| \ll \Delta_{\text{gap}}$ so that edge states are long-lived and have negligible leakage into bulk states on short timescales. After a free-evolving process to perform edge-state operations, we switch off the interaction (second quench), restoring the protection.

Edge-state transfer via local junction interactions. First we consider the simplest case where all the local junction interactions are identical, i.e., $K_i = K$. The system now possesses a D_4 geometric symmetry, with each chain exhibiting inversion symmetry [47], leading to degenerate subspaces of odd-parity eigenstates $|\psi_{l,2n-1}\rangle$, with $n = 1, \ldots, N$. Here, $|\psi_{l,n}\rangle$ denotes the nth eigenstate of SSH chain in ascending order of energy. Consequently, the symmetric edge states $|\psi_{1S}\rangle, |\psi_{2S}\rangle$ become coupled modes owing to their even parity, as shown in Fig. 2(a). In contrast, the antisymmetric states $|\psi_{1A}\rangle, |\psi_{2A}\rangle$ are uncoupled modes. Using the perturbation theory, we obtain the effective interaction Hamiltonian [47]

$$H_{\text{eff}}^{\text{id}} = \widetilde{H}_0 + g(|\psi_{1S}\rangle\langle\psi_{2S}| + \text{H.c.}), \tag{3}$$

where $\widetilde{H}_0 = \sum_{l=1,2}\epsilon_S(|\psi_{lS}\rangle\langle\psi_{lS}| - |\psi_{lA}\rangle\langle\psi_{lA}|)$ is the unperturbed Hamiltonian, with the coupling strength

$$g = 2K\eta^2, \quad \eta = \frac{\sinh[(N+1)\lambda/2]}{\sqrt{2\sum_i \sinh^2[(N+1-i)\lambda]}}. \tag{4}$$

The transition between symmetric edge states results in an oscillation in their subspace, manifesting an edge-state transfer from one chain to another in the coherent evolution. As shown in Fig. 2(b), this leads to the formation of bright and dark interaction channels, where we map the edge states $\{|\psi_{1S}\rangle, |\psi_{1A}\rangle, |\psi_{2A}\rangle, |\psi_{2S}\rangle\}$ as qubit states $\{|\uparrow\uparrow\rangle, |\uparrow\downarrow\rangle, |\downarrow\uparrow\rangle, |\downarrow\downarrow\rangle\}$. In Fig. 2(e), we show an

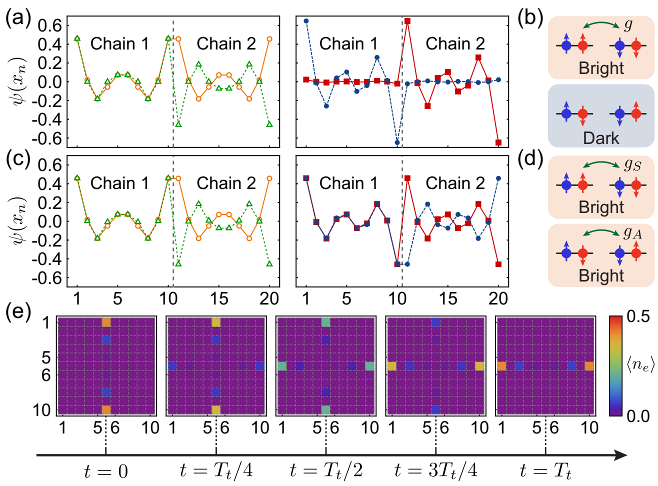

FIG. 2. Junction-induced tunable interactions between edge states with different geometries. Real-space wave functions of the edge states in panels (a) and (c) correspond to D_4 and D_2 symmetries, respectively. Panels (b) and (d) show the schematic illustration of tunable spin-exchange interactions between hybridized edge states. The dark channel opens when the system breaks into D_2 symmetry from D_4 symmetry. Here, we choose the parameters as $J_1 = 0.4J_2$, with $N = 5$ for each chain. The junction interactions are $K_i = 0.07J_2$ in panel (a) and $K_1 = K_3 = 0.07J_2$, $K_2 = K_4 = 0.05J_2$ in panel (c), respectively. (e) Schematic of the edge-state transfer in a coherent evolution, with $T_t = \pi/2g$.

edge-state transfer between different chains with the initial state $|\psi(0)\rangle = |\psi_{1S}\rangle$.

For a less symmetric configuration, with $K_1 = K_4 = K_+$ and $K_2 = K_3 = K_-$ ($K_+ > K_-$), the system retains a D_2 residual symmetry. The effective Hamiltonian in the zero-energy manifold reads

$$H_{\text{eff}}^{\text{rot}} = \widetilde{H}_0 + g_S|\psi_{1S}\rangle\langle\psi_{2S}| + g_A|\psi_{1A}\rangle\langle\psi_{2A}| + \text{H.c.}, \quad (5)$$

where $g_S = \eta^2(K_+ + K_-)$, $g_A = \eta^2(K_+ - K_-)$. Figure 2(c) shows that the edge states are shared by two chains and distribute uniformly at the four edges. The edge states are now denoted by $|\psi_S^+\rangle = (1, 1, 1, 1)^{\text{T}}/2$, $|\psi_S^-\rangle = (1, 1, -1, -1)^{\text{T}}/2$ and $|\psi_A^+\rangle = (1, -1, 1, -1)^{\text{T}}/2$, $|\psi_A^-\rangle = (1, -1, -1, 1)^{\text{T}}/2$ in terms of the basis $\{|\psi_{1L}\rangle, |\psi_{1R}\rangle, |\psi_{2L}\rangle, |\psi_{2R}\rangle\}$. In this configuration, the junction interactions provide an additional interaction channel for the two-qubit exchange process through antisymmetric edge states, as shown in Fig. 2(d). These two interaction channels correspond to two uncoupled qubit-exchange processes. One can control the switching on/off of the interaction channels and their strength by adjusting junction interactions K_i. In a more general case with broken D_2 symmetry, more interaction channels become accessible [47].

Transitions and quantum gates. Having a platform with tunable interactions between four edge states, we investigate its effective model in the picture of two spin qubits. The effective model in the D_2 symmetric scenario has a form of anisotropic Heisenberg Hamiltonian $H_{\text{eff}}^{\text{rot}} = \epsilon_S\sigma_1^z \otimes \sigma_2^z + u\sigma_1^x \otimes \sigma_2^x - v\sigma_1^y \otimes \sigma_2^y$, where $u = \eta^2K_+$, $v = \eta^2K_-$. In the case with D_4 symmetry, it reduces to $u = v$, indicating that the single-spin-flipping

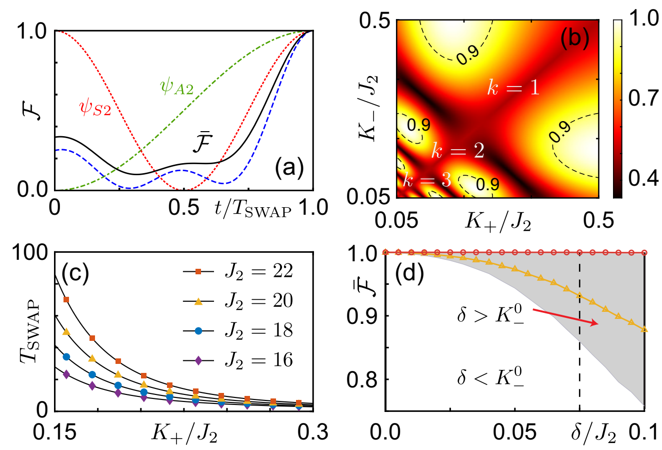

FIG. 3. (a) The gate fidelity of different initial states. The initial states are ψ_{S2}, ψ_{A2}, $(\psi_{S2} + \psi_{A2})/\sqrt{2}$ (blue dashed line), respectively. The solid black line denotes average fidelity $\bar{\mathcal{F}}$. (b) The high-fidelity regions with tunable junction interactions K_i. (c) Tunable gate time by modifying junction interactions with different values of J_2. Here, we set $K_+ = 3K_-$, and J_1 is the optimal value to achieve the highest fidelity. (d) The gate fidelity as a function of the disorder strength δ. The solid lines correspond to the results averaged over 10^3 disorder instances with (red) and without (yellow) the modulation of $K_\pm$, where the shaded area indicates a standard deviation for the yellow line (the fluctuation of the red line is less than 0.01). Here, we take $K_\pm^0$ at $k = 2$ regime, $J_1 = 0.51J_2$, $J_2 = 20$ [except in panel (c)], and $N = 5$.

process $|\uparrow\downarrow\rangle\langle\downarrow\uparrow|$ vanishes. When $u \neq v$, the edge states oscillate in two decoupled subspaces $\Pi : \{|\uparrow\uparrow\rangle, |\downarrow\downarrow\rangle\}$ and $\Sigma : \{|\uparrow\downarrow\rangle, |\downarrow\uparrow\rangle\}$, respectively. We analyze the coherent dynamics of this effective Hamiltonian to illustrate the operation of edge-state qubits, specifically focusing on the SWAP gate [52]. The time evolution of an arbitrary state is given by

$$\psi(t) = \frac{1}{2}\begin{pmatrix} \mathcal{R}_\Pi^+ & 0 & 0 & \mathcal{R}_\Pi^- \\ 0 & \mathcal{R}_\Sigma^+ & \mathcal{R}_\Sigma^- & 0 \\ 0 & \mathcal{R}_\Sigma^- & \mathcal{R}_\Sigma^+ & 0 \\ \mathcal{R}_\Pi^- & 0 & 0 & \mathcal{R}_\Pi^+ \end{pmatrix}\psi(0), \quad (6)$$

where $\mathcal{R}_\Pi^\pm = U_S^+ \pm U_S^-$ and $\mathcal{R}_\Sigma^\pm = U_A^+ \pm U_A^-$ are the matrix elements of different subspaces. The rotating vectors $U_\nu^\pm(t) = e^{-iE_\nu^\pm t/\hbar}(\nu = S, A)$ contribute to oscillations of different components, with energies given by $E_S^\pm = \epsilon_S \pm (u + v)$ and $E_A^\pm = -\epsilon_S \pm (u - v)$. By mapping the matrix elements in Eq. (6) such that $\mathcal{R}_\Pi^+ = \mathcal{R}_\Sigma^- = 2$ and $\mathcal{R}_\Pi^- = \mathcal{R}_\Sigma^+ = 0$, we find that the unitary evolution for edge-state qubits becomes a SWAP gate at the time

$$T_{\text{SWAP}} = \frac{2n\pi}{2(u + v)} = \frac{m\pi}{2(u - v)} = \frac{2k\pi}{2(\epsilon_S + v)}, \quad (7)$$

where $n, m, k \in \mathbb{Z}$. This can be achieved by simply tuning the junction interactions in terms of ϵ_S. As verified by numerical simulations in Fig. 3(a), the SWAP gate is implemented by initializing different states, achieving a gate fidelity of $\bar{\mathcal{F}} > 0.999$ after a complete time cycle of T_{SWAP}. The average fidelity is denoted by $\bar{\mathcal{F}} = \int d\psi_q \text{Tr}\{|\psi_q\rangle\langle\psi_q|\rho(t)\}$, where

ψ_q is the target state. The result is obtained using the total Hamiltonian H_{tot}, which shows good consistency with our analysis based on the effective Hamiltonian $H_{\text{eff}}^{\text{rot}}$. The high fidelity also proves that the edge states barely leak into the bulk during the operation time. Equation (7) determines the sweet point of the junction interactions (K_-^0, K_+^0), with $K_+^0 = 3K_-^0$, $\epsilon_S = 2\eta^2(4k-1)K_-^0$. In Fig. 3(b), the high-fidelity regions are separated by different k values, and the diagram reveals the rotationally symmetric structure by exchanging $K_+ \leftrightarrow K_-$. The gate time can also be tuned by modifying the junction interactions $K_\pm$, as depicted in Fig. 3(c), which scales as $T_{\text{SWAP}} \sim K_+^{-N}$ for K_+ and the fidelity maintains $\bar{\mathcal{F}} > 0.99$ within a certain range of K_+ [47]. Although the edge states are robust to imperfections of J_i (off-diagonal disorder), the quantum gate operations and state transfer are still subject to this disorder since it changes the energy of edge states [14,16] and can result in the breakdown of condition [Eq. (7)]. In our model, the energies of edge states are also related to the junction interactions. Thus, by tuning the junction interactions, we can reconstruct the SWAP gate in Eq. (6) in the presence of the off-diagonal disorder [47]. In Fig. 3(d), we demonstrate the gate fidelity with and without the modulation of $K_\pm$ as a function of the disorder strength δ, where $J_i = J_i + \delta_i$ and the disorder $\delta_i \in [-\delta, \delta]$ is in uniform distribution. The tunable junction interactions significantly reduce the deviation and fluctuation of the fidelity, and it shows a plateau ($\bar{\mathcal{F}} > 0.99$) even when the disorder is larger than the junction interaction K_-^0.

Parity-associated super/subradiance and remote entanglement. In practice, quantum systems are inevitably affected by their environment, and a nonunitary evolution can characterize this process. To make edge-state operations reliable, the dissipative dynamics should be analyzed. Here, we utilize a 1D waveguide to confine the radiative emission from atoms. With this waveguide bath, the collective radiation can suppress the decay of hybridized edge states [53–55]. As shown in Fig. 1(a), each atomic chain couples to an independent waveguide, which induces the dissipative couplings and gives rise to the correlated two-body dissipative dynamics [56–59],

$$\dot{\rho}(t) = -\frac{i}{\hbar}[H_0 + H_{\text{nl}}, \rho(t)] + \mathcal{L}\rho, \tag{8}$$

where $H_{\text{nl}} = \sum_{l=1,2}\sum_{i,j} \hbar g_{ij}(\sigma_{l,i}^+\sigma_{l,j}^- + \sigma_{l,i}^-\sigma_{l,j}^+)$ denotes the nonlocal interaction induced by the exchanging of virtual photons, and the Lindblad superoperator [60–66]

$$\mathcal{L}\rho = \sum_{l=1,2}\sum_{i,j=1}^{2N} \gamma_{ij}\left(\sigma_{li}^-\rho\sigma_{lj}^+ - \frac{1}{2}\sigma_{li}^+\sigma_{lj}^-\rho - \frac{1}{2}\rho\sigma_{li}^+\sigma_{lj}^-\right) \tag{9}$$

shows the correlated decay of the system. The nonlocal interaction and correlated decay are analytically given by [47] $g_{ij} = \gamma_0 \sin(2\pi d_{ij}/\lambda_a)/2$ and $\gamma_{ij} = \gamma_0 \cos(2\pi d_{ij}/\lambda_a)$, respectively, where γ_0 is the spontaneous emission rate to the waveguide bath. The two-body interaction g_{ij} and decay γ_{ij} oscillate with the distance between atoms d_{ij}, scaled by the characteristic wavelength $\lambda_a = 2\pi c/\omega_a$. We assume that the hopping rate J_i is much larger than the atom-field coupling, and thus the interaction term plays a role of disorder. Each atomic chain is carefully designed with bulk atoms spaced by $\lambda_a/2$, while edge atoms are separated from the bulk atoms by $\lambda_a/4$, as shown in Fig. 4(a). In this case, the dissipative dynamics of edge atoms decouples from bulk atoms, leading to parity-associated super/subradiant states. The non-Hermitian Hamiltonian in the single-excitation subspace can be written as

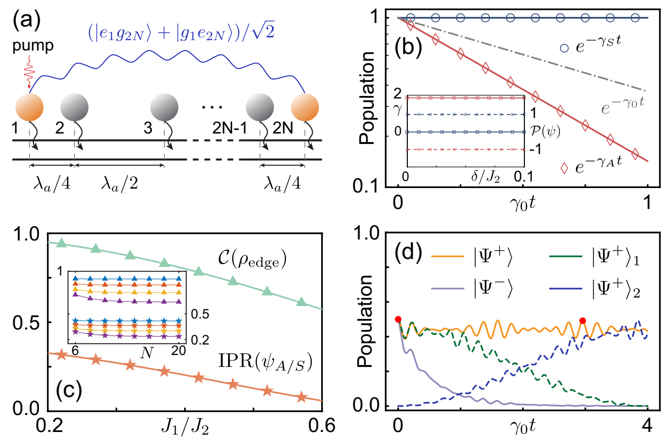

FIG. 4. (a) Schematic of a structured atomic chain coupled to a 1D waveguide. (b) Effective decay rates for hybridized edge states. The inset shows their parity (dashed lines) and decay rates in the presence of disorder. (c) Entanglement of the edge atoms and IPR of edge states. The inset shows their asymptotic limit with N for $J_1/J_2 = 0.3$ (blue), 0.4 (orange), 0.5 (yellow), and 0.6 (purple), respectively. (d) Generation and transfer of the remote entanglement. The solid line indicates the population of Bell states in a single SSH chain, where the red points correspond to concurrence $\mathcal{C}_0 = 0, \mathcal{C}_{\max} = 0.49$. The dashed line shows the transfer of Bell state between two topological chains. Here, $J_1 = 0.25J_2$, $\gamma_0 = 0.035J_2$, $K_i = 0.15J_2$, and $N = 5\,(3)$ for the solid (dashed) lines, respectively.

$$H_{\text{nh}} = H_{\text{SSH}} - i\Gamma_{E,-}|\Gamma_{E,-}\rangle\langle\Gamma_{E,-}| - i\Gamma_B|\Gamma_B\rangle\langle\Gamma_B|, \tag{10}$$

where $|\Gamma_{E,-}\rangle$ and $|\Gamma_B\rangle$ denote the antisymmetric dissipative eigenmodes for the edge and bulk atoms, respectively, with decay rates $\Gamma_{E,-} = 2\gamma_0$ and $\Gamma_B = (2N-2)\gamma_0$. The effective decay rates of the hybridized edge states are given by

$$\gamma_{A/S} = \Gamma_{E,-}|\langle\Gamma_{E,-}|\psi_{A/S}\rangle|^2 + \Gamma_B|\langle\Gamma_B|\psi_{A/S}\rangle|^2, \tag{11}$$

with $\gamma_S = 0$, $\gamma_A \simeq 2\gamma_0$. We investigate the edge-state dynamics by numerically solving the master equation in Eq. (9). As shown in Fig. 4(b), the edge states with odd/even parity exhibit super/subradiance [67–70], where $p_\psi(t) = \text{Tr}(\rho|\psi\rangle\langle\psi|)$. Moreover, in the inset of Fig. 4(b), we demonstrate the topological stability of the super/subradiance when considering the disorder. The parity function is defined as $\mathcal{P}(\psi) = \sum_{j=1}^{N} |\langle\psi|\sigma_j^+|G\rangle + \langle\psi|\sigma_{2N+1-j}^+|G\rangle|^2 - 1$, where $|G\rangle = \otimes_{j=1}^{2N}|g_j\rangle$ and $|g_j\rangle$ denotes the ground state of jth atom. Although the disorder breaks the inversion symmetry, the parity shows robustness since the edge states are protected by chiral symmetry of the SSH chain.

The similarity between highly localized edge states and Bell states $|\Psi^\pm\rangle = (|e_1 g_{2N}\rangle \pm |g_1 e_{2N}\rangle)/\sqrt{2}$ enables the generation of remote entangled states, where $|e_j\rangle$ is the excited state of jth atom. By tracing out the bulk atoms, we investigate the concurrence $\mathcal{C}$ of the reduced density matrix ρ_{edge} of edge states. Figure 4(c) displays the concurrence and the inverse participation ratio (IPR) of two edge atoms as functions of J_1/J_2, where the IPR measures the localization of wave functions, denoted by $\mathrm{IPR}(\psi) = \sum_i |\psi(r_i)|^4 = \sum_i p_i^2$, with p_i being the probability at ith site. As the cell number N increases, they exhibit asymptotic independence [47]. To prepare a remote entangled state, one can first excite an edge atom using a pump field, as depicted in Fig. 4(a). The entangled state $|\Psi^-\rangle$ then decays rapidly, while $|\Psi^+\rangle$ shows slight oscillations with other nonradiative states with a mean concurrence $\bar{\mathcal{C}} \simeq 0.5|\langle\psi_S|\Psi^+\rangle|^4$, as shown in Fig. 4(d). Since the remote entanglement is attached to the symmetric edge state, it inherits the topological protection and is insensitive to the atomic dissipation. Further, assisted with the junction interactions, in Fig. 4(d) we demonstrate the robust entanglement transfer between two chains.

Conclusion. In summary, we have proposed a topological system for studying controllable interactions via a local junction. The dynamics is constrained in the zero-energy manifold, providing two interacting subspaces for transitions of edge states. By tuning the junction interactions with D_4 and D_2 geometric symmetries, we find different interaction channels between edge states. According to the theory, we implement the robust quantum state transfer and SWAP gate for the topological system, which suggests the excellent approximation from total Hamiltonian to the effective spin model. In addition to coherent dynamics, this system could support edge states that are insensitive to environmental dissipation, thus protecting them from both disorder and decoherence. Our work paves the way toward controlling topological edge states with few-body local interactions in a coherent evolution.

Acknowledgments. We thank Y.-X. Liu, J.-Q. Liao, and Z. Peng for stimulating discussions. This work was supported by the National Natural Science Foundation of China (Grants No. 12375025 and No. 11874432) and the National Key R&D Program of China (Grant No. 2019YFA0308200).

Data availability. The data that support the findings of this article are not publicly available. The data are available from the authors upon reasonable request.

[1] M. Z. Hasan and C. L. Kane, *Colloquium:* Topological insulators, Rev. Mod. Phys. **82**, 3045 (2010).

[2] X.-L. Qi and S.-C. Zhang, Topological insulators and superconductors, Rev. Mod. Phys. **83**, 1057 (2011).

[3] B. I. Halperin, Quantized Hall conductance, current-carrying edge states, and the existence of extended states in a two-dimensional disordered potential, Phys. Rev. B **25**, 2185 (1982).

[4] Q. Niu and D. J. Thouless, Quantised adiabatic charge transport in the presence of substrate disorder and many-body interaction, J. Phys. A: Math. Gen. **17**, 2453 (1984).

[5] M. Büttiker, Absence of backscattering in the quantum Hall effect in multiprobe conductors, Phys. Rev. B **38**, 9375 (1988).

[6] M. Hafezi, E. A. Demler, M. D. Lukin, and J. M. Taylor, Robust optical delay lines with topological protection, Nat. Phys. **7**, 907 (2011).

[7] J. Perczel, J. Borregaard, D. E. Chang, H. Pichler, S. F. Yelin, P. Zoller, and M. D. Lukin, Topological quantum optics in two-dimensional atomic arrays, Phys. Rev. Lett. **119**, 023603 (2017).

[8] M. A. Bandres, S. Wittek, G. Harari, M. Parto, J. Ren, M. Segev, D. N. Christodoulides, and M. Khajavikhan, Topological insulator laser: Experiments, Science **359**, eaar4005 (2018).

[9] S. Ryu and Y. Hatsugai, Topological origin of zero-energy edge states in particle-hole symmetric systems, Phys. Rev. Lett. **89**, 077002 (2002).

[10] J. K. Asbóth, L. Oroszlány, and A. Pályi, *A Short Course on Topological Insulators* (Springer International Publishing, Cham, 2016).

[11] W. Nie and Y.-X. Liu, Bandgap-assisted quantum control of topological edge states in a cavity, Phys. Rev. Res. **2**, 012076(R) (2020).

[12] N. Y. Yao, C. R. Laumann, A. V. Gorshkov, H. Weimer, L. Jiang, J. I. Cirac, P. Zoller, and M. D. Lukin, Topologically protected quantum state transfer in a chiral spin liquid, Nat. Commun. **4**, 1585 (2013).

[13] C. Dlaska, B. Vermersch, and P. Zoller, Robust quantum state transfer via topologically protected edge channels in dipolar arrays, Quantum Sci. Technol. **2**, 015001 (2017).

[14] N. Lang and H. P. Büchler, Topological networks for quantum communication between distant qubits, npj Quantum Inf. **3**, 47 (2017).

[15] F. Mei, G. Chen, L. Tian, S.-L. Zhu, and S. Jia, Robust quantum state transfer via topological edge states in superconducting qubit chains, Phys. Rev. A **98**, 012331 (2018).

[16] S. Longhi, G. L. Giorgi, and R. Zambrini, Landau–Zener topological quantum state transfer, Adv. Quantum Technol. **2**, 1800090 (2019).

[17] F. M. D'Angelis, F. A. Pinheiro, D. Guéry-Odelin, S. Longhi, and F. Impens, Fast and robust quantum state transfer in a topological Su-Schrieffer-Heeger chain with next-to-nearest-neighbor interactions, Phys. Rev. Res. **2**, 033475 (2020).

[18] L. Qi, Y. Yan, Y. Xing, X.-D. Zhao, S. Liu, W.-X. Cui, X. Han, S. Zhang, and H.-F. Wang, Topological router induced via long-range hopping in a Su-Schrieffer-Heeger chain, Phys. Rev. Res. **3**, 023037 (2021).

[19] J. Alicea, Y. Oreg, G. Refael, F. von Oppen, and M. P. A. Fisher, Non-Abelian statistics and topological quantum information processing in 1D wire networks, Nat. Phys. **7**, 412 (2011).

[20] S. D. Sarma, M. Freedman, and C. Nayak, Majorana zero modes and topological quantum computation, npj Quantum Inf. **1**, 15001 (2015).

[21] T. Karzig, C. Knapp, R. M. Lutchyn, P. Bonderson, M. B. Hastings, C. Nayak, J. Alicea, K. Flensberg, S. Plugge, Y. Oreg, C. M. Marcus, and M. H. Freedman, Scalable designs for quasiparticle-poisoning-protected topological quantum computation with Majorana zero modes, Phys. Rev. B **95**, 235305 (2017).

[22] I. Brouzos, I. Kiorpelidis, F. K. Diakonos, and G. Theocharis, Fast, robust, and amplified transfer of topological edge modes

on a time-varying mechanical chain, Phys. Rev. B **102**, 174312 (2020).

[23] T. Tian, Y. Zhang, L. Zhang, L. Wu, S. Lin, J. Zhou, C.-K. Duan, J.-H. Jiang, and J. Du, Experimental realization of nonreciprocal adiabatic transfer of phonons in a dynamically modulated nanomechanical topological insulator, Phys. Rev. Lett. **129**, 215901 (2022).

[24] P. Pakkiam, N. P. Kumar, M. Pletyukhov, and A. Fedorov, Qubit-controlled directional edge states in waveguide QED, npj Quantum Inf. **9**, 53 (2023).

[25] D. J. Thouless, Quantization of particle transport, Phys. Rev. B **27**, 6083 (1983).

[26] M. Lohse, C. Schweizer, O. Zilberberg, M. Aidelsburger, and I. Bloch, A Thouless quantum pump with ultracold bosonic atoms in an optical superlattice, Nat. Phys. **12**, 350 (2016).

[27] S. Nakajima, T. Tomita, S. Taie, T. Ichinose, H. Ozawa, L. Wang, M. Troyer, and Y. Takahashi, Topological Thouless pumping of ultracold fermions, Nat. Phys. **12**, 296 (2016).

[28] X. Gu, S. Chen, and Y.-X. Liu, Topological edge states and pumping in a chain of coupled superconducting qubits, arXiv:1711.06829.

[29] S. Longhi, Topological pumping of edge states via adiabatic passage, Phys. Rev. B **99**, 155150 (2019).

[30] Y. E. Kraus, Y. Lahini, Z. Ringel, M. Verbin, and O. Zilberberg, Topological states and adiabatic pumping in quasicrystals, Phys. Rev. Lett. **109**, 106402 (2012).

[31] M. Verbin, O. Zilberberg, Y. Lahini, Y. E. Kraus, and Y. Silberberg, Topological pumping over a photonic Fibonacci quasicrystal, Phys. Rev. B **91**, 064201 (2015).

[32] O. Zilberberg, S. Huang, J. Guglielmon, M. Wang, K. P. Chen, Y. E. Kraus, and M. C. Rechtsman, Photonic topological boundary pumping as a probe of 4D quantum Hall physics, Nature (London) **553**, 59 (2018).

[33] Q. Cheng, H. Wang, Y. Ke, T. Chen, Y. Yu, Y. S. Kivshar, C. Lee, and Y. Pan, Asymmetric topological pumping in nonparaxial photonics, Nat. Commun. **13**, 249 (2022).

[34] M. I. N. Rosa, R. K. Pal, J. R. F. Arruda, and M. Ruzzene, Edge states and topological pumping in spatially modulated elastic lattices, Phys. Rev. Lett. **123**, 034301 (2019).

[35] I. H. Grinberg, M. Lin, C. Harris, W. A. Benalcazar, C. W. Peterson, T. L. Hughes, and G. Bahl, Robust temporal pumping in a magneto-mechanical topological insulator, Nat. Commun. **11**, 974 (2020).

[36] Y. Xia, E. Riva, M. I. N. Rosa, G. Cazzulani, A. Erturk, F. Braghin, and M. Ruzzene, Experimental observation of temporal pumping in electromechanical waveguides, Phys. Rev. Lett. **126**, 095501 (2021).

[37] W. Cheng, E. Prodan, and C. Prodan, Experimental demonstration of dynamic topological pumping across incommensurate bilayered acoustic metamaterials, Phys. Rev. Lett. **125**, 224301 (2020).

[38] Z.-G. Chen, W. Tang, R.-Y. Zhang, Z. Chen, and G. Ma, Landau-Zener transition in the dynamic transfer of acoustic topological states, Phys. Rev. Lett. **126**, 054301 (2021).

[39] H. Chen, H. Zhang, Q. Wu, Y. Huang, H. Nguyen, E. Prodan, X. Zhou, and G. Huang, Creating synthetic spaces for higher-order topological sound transport, Nat. Commun. **12**, 5028 (2021).

[40] V. Lahtinen and J. K. Pachos, A short introduction to topological quantum computation, SciPost Phys. **3**, 021 (2017).

[41] P. Boross, J. K. Asbóth, G. Széchenyi, L. Oroszlány, and A. Pályi, Poor man's topological quantum gate based on the Su-Schrieffer-Heeger model, Phys. Rev. B **100**, 045414 (2019).

[42] M. S. Scheurer and A. Shnirman, Nonadiabatic processes in Majorana qubit systems, Phys. Rev. B **88**, 064515 (2013).

[43] L. Privitera, A. Russomanno, R. Citro, and G. E. Santoro, Nonadiabatic breaking of topological pumping, Phys. Rev. Lett. **120**, 106601 (2018).

[44] P. Delplace, D. Ullmo, and G. Montambaux, Zak phase and the existence of edge states in graphene, Phys. Rev. B **84**, 195452 (2011).

[45] W. P. Su, J. R. Schrieffer, and A. J. Heeger, Solitons in polyacetylene, Phys. Rev. Lett. **42**, 1698 (1979).

[46] Z.-L. Xiang, S. Ashhab, J. Q. You, and F. Nori, Hybrid quantum circuits: Superconducting circuits interacting with other quantum systems, Rev. Mod. Phys. **85**, 623 (2013).

[47] See Supplemental Material at http://link.aps.org/supplemental/10.1103/ylrq-98wl for details, including the derivation of the effective Hamiltonian based on symmetry analysis and photon-mediated super/subradiance of edge states, the evaluation of the SWAP gate, the remote entanglement generation protocol, and a brief discussion about the experimental implementation in superconducting circuits.

[48] J. C. Y. Teo, A. P. Schnyder, and S. Ryu, Classification of topological quantum matter with symmetries, Rev. Mod. Phys. **88**, 035005 (2016).

[49] O. Viyuela, A. Rivas, and M. A. Martin-Delgado, Uhlmann phase as a topological measure for one-dimensional fermion systems, Phys. Rev. Lett. **112**, 130401 (2014).

[50] J. C. Budich and S. Diehl, Topology of density matrices, Phys. Rev. B **91**, 165140 (2015).

[51] B. Monserrat and D. Vanderbilt, Temperature effects in the band structure of topological insulators, Phys. Rev. Lett. **117**, 226801 (2016).

[52] Y. P. Kandel, H. Qiao, S. Fallahi, G. C. Gardner, M. J. Manfra, and J. M. Nichol, Coherent spin-state transfer via Heisenberg exchange, Nature (London) **573**, 553 (2019).

[53] M. Bello, G. Platero, J. I. Cirac, and A. González-Tudela, Unconventional quantum optics in topological waveguide QED, Sci. Adv. **5**, eaaw0297 (2019).

[54] W. Nie, Z. H. Peng, F. Nori, and Y.-x. Liu, Topologically protected quantum coherence in a superatom, Phys. Rev. Lett. **124**, 023603 (2020).

[55] C. McDonnell and B. Olmos, Subradiant edge states in an atom chain with waveguide-mediated hopping, Quantum **6**, 805 (2022).

[56] W. Nie, M. Antezza, Y.-x. Liu, and F. Nori, Dissipative topological phase transition with strong system-environment coupling, Phys. Rev. Lett. **127**, 250402 (2021).

[57] R. H. Lehmberg, Radiation from an *N*-atom system. I. General formalism, Phys. Rev. A **2**, 883 (1970).

[58] H. T. Dung, L. Knöll, and D.-G. Welsch, Resonant dipole-dipole interaction in the presence of dispersing and absorbing surroundings, Phys. Rev. A **66**, 063810 (2002).

[59] Z. Ficek and R. Tanaś, Entangled states and collective nonclassical effects in two-atom systems, Phys. Rep. **372**, 369 (2002).

[60] F. Le Kien, S. D. Gupta, K. P. Nayak, and K. Hakuta, Nanofiber-mediated radiative transfer between two distant atoms, Phys. Rev. A **72**, 063815 (2005).

[61] A. Gonzalez-Tudela, D. Martin-Cano, E. Moreno, L. Martin-Moreno, C. Tejedor, and F. J. Garcia-Vidal, Entanglement of two qubits mediated by one-dimensional plasmonic waveguides, Phys. Rev. Lett. **106**, 020501 (2011).

[62] D. E. Chang, L. Jiang, A. V. Gorshkov, and H. J. Kimble, Cavity QED with atomic mirrors, New J. Phys. **14**, 063003 (2012).

[63] K. Lalumière, B. C. Sanders, A. F. van Loo, A. Fedorov, A. Wallraff, and A. Blais, Input-output theory for waveguide QED with an ensemble of inhomogeneous atoms, Phys. Rev. A **88**, 043806 (2013).

[64] P. Doyeux, S. A. H. Gangaraj, G. W. Hanson, and M. Antezza, Giant interatomic energy-transport amplification with nonreciprocal photonic topological insulators, Phys. Rev. Lett. **119**, 173901 (2017).

[65] M. Mirhosseini, E. Kim, X. Zhang, A. Sipahigil, P. B. Dieterle, A. J. Keller, A. Asenjo-Garcia, D. E. Chang, and O. Painter, Cavity quantum electrodynamics with atom-like mirrors, Nature (London) **569**, 692 (2019).

[66] P. Y. Wen, K.-T. Lin, A. F. Kockum, B. Suri, H. Ian, J. C. Chen, S. Y. Mao, C. C. Chiu, P. Delsing, F. Nori, G.-D. Lin, and I.-C. Hoi, Large collective Lamb shift of two distant superconducting artificial atoms, Phys. Rev. Lett. **123**, 233602 (2019).

[67] A. F. van Loo, A. Fedorov, K. Lalumière, B. C. Sanders, A. Blais, and A. Wallraff, Photon-mediated interactions between distant artificial atoms, Science **342**, 1494 (2013).

[68] A. Asenjo-Garcia, J. D. Hood, D. E. Chang, and H. J. Kimble, Atom-light interactions in quasi-one-dimensional nanostructures: A Green's-function perspective, Phys. Rev. A **95**, 033818 (2017).

[69] Y.-X. Zhang and K. Mølmer, Theory of subradiant states of a one-dimensional two-level atom chain, Phys. Rev. Lett. **122**, 203605 (2019).

[70] M. Zanner, T. Orell, C. M. F. Schneider, R. Albert, S. Oleschko, M. L. Juan, M. Silveri, and G. Kirchmair, Coherent control of a multi-qubit dark state in waveguide quantum electrodynamics, Nat. Phys. **18**, 538 (2022).